Inorganic Chemistry
Article

Inorg. Chem. **2010**, *49*, 4901–4908 **4901**
DOI: 10.1021/ic9024958

Interaction of Thioether Groups at the Open Coordination Sites of Palladium(II) and Platinum(II) Complexes Probed by Luminescence Spectroscopy at Variable Pressure

Esther Pierce,[†] Etienne Lanthier,[†] Caroline Genre,[†] Yurii Chumakov,[‡] Dominique Luneau,[‡] and Christian Reber*[,†]

[†]*Département de Chimie, Université de Montréal, Montréal QC H3C 3J7, Canada, and* [‡]*Université Claude Bernard Lyon 1, Laboratoire des Multimatériaux et Interfaces (UMR 5615), Campus de La Doua, 69622 Villeurbanne Cedex, France*

Received December 16, 2009

The crystal structures of $[PtCl_2(ttcn)]$, $[PdCl_2(ttcn)]$, $[Pt(ethylenediamine)(ttcn)](PF_6)_2$, and $[Pd(ethylenediamine)(ttcn)](PF_6)_2$ (ttcn = 1,4,7-trithiacyclononane) show short apical metal—S(ttcn) distances, qualitatively indicating an interaction. Luminescence spectroscopy was used to study these crystalline complexes at room temperature and variable hydrostatic pressure. The luminescence band maximum of $[PdCl_2(ttcn)]$ shows a pressure-induced blue shift of $+6\ cm^{-1}$/kbar, while the platinum(II) compounds show a red shift of approximately $-20\ cm^{-1}$/kbar. This difference is rationalized in terms of a competition between blue shifts due to pressure-induced metal−ligand bond shortening in the equatorial plane and increasing out-of-plane distance of the metal center, and a red shift due to the approach of the apical sulfur donor to the metal center. Density functional theory (DFT) calculations indicate d-d luminescence transitions and a different nature of the highest occupied molecular orbital (HOMO) for $[PdCl_2(ttcn)]$ than for $[PtCl_2(ttcn)]$, while the lowest unoccupied molecular orbitals (LUMOs) are identical in character. This electronic structure difference is used to rationalize the different pressure effects.

1. Introduction

The interaction of a pendant nucleophile with the metal center at a vacant axial site of a square-planar d^8 complex can have a distinct influence on its electronic structure and reactivity.[1−3] Cyclic ligands such as 1,4,7-trithiacyclononane (ttcn) have been used to provide the pendant nucleophile, and the ligands completing the square-planar coordination sphere lead to a variation of the distance between the metal center and the pendant nucleophile.[2] External pressure has been shown to significantly vary this distance, for example, a decrease by 0.2 Å has been recently reported for $[Pd(ttcn)Cl_2]$ between ambient pressure and 45 kbar.[4]

Luminescence spectroscopy provides quantitative insight on the electronic structure of a wide variety of square-planar luminophores. The nature of the emitting state of many platinum(II) complexes can be chemically controlled via the electronic structure of the ligands, and luminescence spectroscopy has been very successfully applied to characterize the lowest-energy excited state.[5−11] Spectra measured as a function of pressure have been reported and show a blue shift of the band maxima on the order of $+20\ cm^{-1}$/kbar to $+30\ cm^{-1}$/kbar for d-d transitions.[12−15] In the presence of strong axial interactions, such as stacked structures, the luminescence maxima show a pronounced red shift with increasing pressure.[16] These variations are continuous and reversible, providing important trends and insight on the magnitude of different interactions. Pressure-dependent

*To whom correspondence should be addressed. E-mail: christian.reber@umontreal.ca. Fax: (+1) 514-343-7586.

(1) Blake, A. J.; Roberts, Y. V.; Schröder, M. *Dalton Trans.* **1996**, 1885.
(2) Green, T. W.; Lieberman, R.; Mitchell, N.; Krause Bauer, J. A.; Connick, W. B. *Inorg. Chem.* **2005**, *44*, 1955.
(3) Nikol, H.; Bürgi, H.-B.; Hardcastle, K. I.; Gray, H. B. *Inorg. Chem.* **1995**, *34*, 6319.
(4) Allan, D. R.; Blake, A. J.; Huang, D.; Prior, T. J.; Schröder, M. *Chem. Commun.* **2006**, 4081.
(5) Shikhova, E.; Danilov, E. O.; Kinayyigit, S.; Pomestchenko, I. E.; Tregubov, A. D.; Camerel, F.; Retailleau, P.; Ziessel, R.; Castellano, F. N. *Inorg. Chem.* **2007**, *46*, 3038.
(6) Muro, M. L.; Diring, S.; Wang, X.; Ziessel, R.; Castellano, F. N. *Inorg. Chem.* **2008**, *47*, 6796.
(7) Clark, M. L.; Diring, S.; Retailleau, P.; McMillin, D. R.; Ziessel, R. *Chem.—Eur. J.* **2008**, *14*, 7168.
(8) Wen, H.-M.; Wu, Y.-H.; Fan, Y.; Zhang, L.-Y.; Chen, C.-N.; Chen, Z.-N. *Inorg. Chem.* **2010**, *49*, 2210.
(9) Ji, Z.; Li, S.; Li, Y.; Sun, W. *Inorg. Chem.* **2010**, *49*, 1337.
(10) Schneider, J.; Du, P.; Wang, X.; Brennessel, W. W.; Eisenberg, R. *Inorg. Chem.* **2009**, *48*, 1498.
(11) Ji, Z.; Azenkeng, A.; Hoffmann, M.; Sun, W. *Dalton Trans.* **2009**, 7725.
(12) Genre, C.; Levasseur-Theriault, G.; Reber, C. *Can. J. Chem.* **2009**, *87*, 1625.
(13) Grey, J. K.; Butler, I. S.; Reber, C. *J. Am. Chem. Soc.* **2002**, *224*, 9384.
(14) Grey, J. K.; Butler, I. S.; Reber, C. *Inorg. Chem.* **2003**, *42*, 6503.
(15) Hidvegi, I.; Tuszynski, W.; Gliemannn, G. *Chem. Phys. Lett.* **1981**, *77*, 517.
(16) Gliemann, G.; Yersin, H. *Struct. Bonding* (*Berlin*) **1985**, *62*, 87.

Published on Web 05/11/2010

luminescence spectroscopy[17] is therefore complementary to the chemical variation of the coordination sphere through ligand substitution. The strength of the axial interaction can be probed experimentally, and the results compared to literature data for isoelectronic square-planar compounds without pendant nucleophiles. d-d transitions are the most straightforward to compare with electronic structure models, and pressure-dependent luminescence spectra of three complexes are presented and analyzed in the following. Density functional theory (DFT) calculations are used to interpret the results and to identify significant differences of their electronic structure.

2. Experimental Section

All reagents and solvents were purchased from the Sigma-Aldrich company and used without further purification.

Synthesis of [Pd(ttcn)en](PF$_6$)$_2$. On the basis of the procedure by Nikol et al.[3] Pd(en)Cl$_2$ (67 mg, 0.28 mmol) and 1,4,7-trithiacyclononane (51 mg, 0.28 mmol) were refluxed for 3 h under argon in a 1:1:1 mixture of water, acetonitrile, and methanol (30 mL). The solution turned intense red. After cooling, an excess (10 equiv) of NH_4PF_6 was added to the solution, and the solvent was partially removed. The solution was placed in a refrigerator overnight, and red crystals precipitated. They were washed with water to remove traces of solid NH_4PF_6 and dried in vacuo. Elemental analysis calculated for $C_8H_{18}N_2S_3P_2F_{12}Pd$ (634.79): C 15.14, H 2.86, N 4.41, S 15.15; found: C 15.12, H 3.46, N 4.30, S 14.71; ^{1}H NMR (300 MHz, CD_3CN): δ 4.32 (bs, 2H, NH), 3.20 (m, 6H, interior ttcn H), 3.04 (m, 6H, exterior ttcn H), 2.88 (sept, 4H, CH_2). ^{13}C NMR (300 MHz, CD_3CN): δ 48.1, 35.0 .

Synthesis of [Pt(ttcn)en](PF$_6$)$_2$. Pt(en)Cl$_2$ was prepared according to a procedure by Ellis et al.[18] Pt(en)Cl$_2$ (185 mg, 0.5 mmol) and 1,4,7-trithiacyclononane (103 mg, 0.57 mmol) were refluxed in a 1:1:1 mixture of water, acetonitrile, and methanol (75 mL) under argon for 3.5 h. After cooling to room temperature, an excess of NH_4PF_6 was added. The solution was concentrated to 25 mL, filtered, and left in the refrigerator overnight. Yellow crystals precipitated and were collected and washed with ice cold ethanol and ether. Elemental analysis calculated for $C_8H_{18}N_2S_3P_2F_{12}Pt$ (723.45): C 13.28, H 2.51, N 3.87, S 13.30; found: C 13.99, H 2.20, N 3.78, S 13.73; ^{1}H NMR (300 MHz, CD_3CN): δ 4.83 (bs, 2H, NH), 3.15−2.86 (m, 12 H, ttcn), 2.80 (m, 4H, CH_2, J^3_{Pt-H} = 19.6 Hz); ^{13}C NMR (300 MHz, CD_3CN): δ 48.6, 34.8.

Synthesis of [Pd(ttcn)Cl$_2$] and [Pt(ttcn)Cl$_2$]. [Pd(ttcn)Cl$_2$] was prepared according to a published procedure.[1] Elemental analysis calculated for $C_6H_{12}S_3Cl_2Pd$ (357.68): C 20.15, H 3.38, S 26.89; found: C 20.08, H 3.22, S 26.10. [Pt(ttcn)Cl$_2$] was prepared according to a published procedure.[19] Raman spectrum: 191, 226, 266, 323, 352, 381, 412, 604, 628, 637, 668, 689, 699 cm^{-1}. Crystal structures for [Pd(ttcn)Cl$_2$] and [Pt(ttcn)Cl$_2$] have been published.[19,20]

Single-Crystal X-ray Diffraction. X-ray crystallographic data for [Pd(ttcn)en](PF$_6$)$_2$ and [Pt(ttcn)en](PF$_6$)$_2$ were collected from single crystal samples, which were mounted on a loop fiber. Data were collected using a Bruker Platform diffractometer, equipped with a Bruker SMART 2K Charged-Coupled Device (CCD) Area Detector using the program SMART and normal focus sealed tube source graphite monochromatic Cu−K$_\alpha$ radiation. The crystal-to-detector distance was 4.908 cm, and the data collection was carried out in 512 × 512 pixel mode, utilizing 4 × 4 pixel binning. The initial unit cell parameters were determined by a least-squares fit of the angular setting of strong reflections, collected by a 9.0 degree scan in 30 frames over four different parts of the reciprocal space (120 frames total). One complete sphere of data was collected, to better than 0.8% resolution. Upon completion of the data collection, the first 101 frames were recollected to improve the decay correction analysis.

All non-H atoms were refined by full-matrix least-squares with anisotropic displacement parameters. The H atoms were generated geometrically (C−H 0.97 Å and N−H 0.86 Å) and were included in the refinement in the riding model approximation; their temperature factors were set to 1.2 times those of the equivalent isotropic temperature factors of the parent site. A final verification of possible voids was performed using the VOID routine of the PLATON program.[21]

Spectroscopic Measurements. The luminescence and Raman measurements were carried out using a Renishaw inVia imaging microscope system equipped with a CCD camera. Excitation sources were a 488 nm argon ion laser for the luminescence experiments and a 633 nm He−Ne laser for the Raman experiments. All spectra are unpolarized and corrected for spectrometer response. Pressure was applied to the solid samples by loading crystals into a gasketed diamond-anvil cell (DAC, High-Pressure Diamond Optics). The ruby (R_1) method was used to calibrate the pressure,[22] with paraffin oil used as the pressure transmitting medium. All pressure effects reported here are reversible: upon gradual release of external pressure, all quantities return to their normal values at ambient pressure. For the temperature-dependent measurements, the samples were cooled in a Linkam microscope cryostat system by pumping off liquid nitrogen. The absorption spectrum of [Pt(ttcn)en](PF$_6$)$_2$ in solution was recorded with a Varian Cary 5E double beam UV−visible spectrophotometer.

DFT Calculations. DFT calculations for [Pd(ttcn)Cl$_2$] and [Pt(ttcn)Cl$_2$] were made with the Gaussian 03 program package.[23] Crystallographic atom coordinates[4,19] were used as a starting point and first optimized with the SVWN local approximation, followed by the PBE functional for tighter geometry optimization.

The SIESTA code has been used to calculate pressure-dependent structural changes and the variation of the HOMO−LUMO gap in crystalline [Pd(ttcn)Cl$_2$] and [Pt(ttcn)Cl$_2$]. This is a special situation, as calculated structures can be compared to the published experimental structure of [Pd(ttcn)Cl$_2$] at a number of different pressures.[4] We have performed DFT calculations using the SIESTA method,[24] which is based on pseudopotentials and numerical localized atomic orbitals as basis sets. The calculations were performed using the generalized gradient approximation (GGA) with the PBE scheme.[25] Core electrons were replaced by

(17) Bray, K. L. *Top. Curr. Chem.* **2001**, *213*, 1.
(18) Ellis, L. T.; Er, H. M.; Hambley, T. W. *Aust. J. Chem.* **1995**, *48*, 793.
(19) Grant, G. J.; Brandow, C. G.; Galas, D. F.; Davis, J. P.; Pennington, W. T.; Valente, E. J.; Zubkowski, J. D. *Polyhedron* **2001**, *20*, 3333.
(20) Blake, A. J.; Holder, A. J.; Roberts, Y. V.; Schröder, M. *Acta Crystallogr.* **1988**, *C44*, 360.
(21) Spek, A. L. *Platon*, 2000 version; University of Utrecht: Utrecht, The Netherlands, 2000.
(22) Piermarini, G. J.; Block, S.; Barnett, J. D.; Forman, R. A. *J. Appl. Phys.* **1975**, *46*, 2774.
(23) Frisch, M. J.; Trucks, G. W.; Schlegel, H. B.; Scuseria, G. E.; Robb, M. A.; Cheeseman, J. R.; Zakrzewski, V. G.; Montgomery, Jr., J. A.; Stratmann, R. E.; Burant, J. C.; Dapprich, S.; Millam, J. M.; Daniels, A. D.; Kudin, K. N.; Strain, M. C.; Farkas, O.; Tomasi, J.; Barone, V.; Mennucci, B.; Cossi, M.; Adamo, C.; Jaramillo, J.; Cammi, R.; Pomelli, C.; Ochterski, J.; Petersson, G. A.; Ayala, P. Y.; Morokuma, K.; Malick, D. K.; Rabuck, A. D.; Raghavachari, K.; Foresman, J. B.; Ortiz, J. V.; Cui, Q.; Baboul, A. G.; Clifford, S.; Cioslowski, J.; Stefanov, B. B.; Liu, G.; Liashenko, A.; Piskorz, P.; Komaromi, I.; Gomperts, R.; Martin, R. L.; Fox, D. J.; Keith, T.; Al-Laham, M. A.; Peng, C. Y.; Nanayakkara, A.; Challacombe, M.; Gill, P. M. W.; Johnson, B.; Chen, W.; Wong, M. W.; Andres, J. L.; Gonzalez, C.; Head-Gordon, M.; Replogle, E. S.; Pople, J. A. *Gaussian 03*, Development Version (Revision A.01); Gaussian, Inc.: Pittsburgh, PA, 2003.
(24) Soler, J. M.; Artacho, E.; Gale, J. D.; Garcia, A.; Junquera, J.; Ordejon, P.; Sanchez-Portal, D. *J. Phys.: Condens. Matter* **2002**, *14*, 2745.
(25) Perdew, J. P.; Burke, K.; Ernzerhof, M. *Phys. Rev. Lett.* **1996**, *77*, 3865.

Table 1. Crystallographic Data for $[Pd(ttcn)en](PF_6)_2$ and $[Pt(ttcn)en](PF_6)_2$[a]

	$[Pd(ttcn)en](PF_6)_2$	$[Pt(ttcn)en](PF_6)_2$
empirical formula	$C_8H_{18}N_2S_3P_2F_{12}Pd$	$C_8H_{18}N_2S_3P_2F_{12}Pt$
M	634.76	723.45
system	monoclinic	orthorhombic
space group	$P2_1/c$	$Pbca$
a [Å]	6.547(1)	16.9954(5)
b [Å]	19.9066(4)	12.3930(4)
c [Å]	16.1215(4)	39.366(1)
B [deg]	90.676(1)	90
V [Å^3]	2098.92(7)	8291.4(4)
Z	4	16
T [°C]	293(2)	293(2)
λ [Å]	1.54178	1.54178
$\mu(Cu_{K\alpha})$ [mm^{-1}]	12.373	17.97
$F(000)$	1248	5504
θ range [deg]	3.53−71.58	3.44−71.99
independent reflections	4082	8145
independent reflections with $I > 2\sigma(I)$	3231	6765
$R[F^2 > 2\sigma(F)^2]$	0.043	0.047
$\omega R_2(F^2)$	0.104	0.12

[a]Estimated standard deviation in the least significant digits are given in parentheses.

norm-conserving pseudopotentials using the scalar-relativistic Troullier−Martins scheme[26] in the Kleinman−Bylander factorized form[27] with nonlinear core corrections.[28] We used the target-pressure-molecular-dynamics technique with variable cell shape and coordinate optimization by conjugate gradients as provided within the SIESTA code to calculate the crystal structures of $[Pd(ttcn)Cl_2]$ and $[Pt(ttcn)Cl_2]$. The hydrostatic pressure was varied at room temperature from 13 kbar to 36 kbar. Full geometry relaxation calculations of experimental structures of $[Pd(ttcn)Cl_2]$ and $[Pt(ttcn)Cl_2]$ were performed before the target-pressure-molecular-dynamics simulations.

3. Results

3.1. Crystal Structure of $[Pd(ttcn)en](PF_6)_2$. The single crystal X-ray diffraction of $[Pd(ttcn)en](PF_6)_2$ was determined at 293 K. The compound crystallizes in the $P2_1/c$ group, with $Z = 4$. Table 1 provides further information about the unit cell. The approximately square-planar coordination sphere of the Pd atom is formed by two N atoms of the ethylenediamine ligand and two S atoms of the 1,4,7-trithiacyclononane (ttcn) ligand. The ligand adopts an endodentate geometry, allowing the third sulfur atom to have a weak apical interaction with the metal atom, leading to a $Pd-S_{apical}$ distance of 3.00 Å. This results effectively in a five-coordinate metal center, as shown in the Supporting Information, Figure S1. The C atoms of the ethylenediamine ligand are disordered and resolved into two orientations, with occupancy factors of 0.5 on each position, as both are hexafluorophosphate anions. The complex molecules and hexafluorophosphate anions pack as discrete units, and no significant intermolecular interaction is observed.

The equatorial Pd−S distances are 2.257 and 2.253 Å, and the Pd−N distances 2.08 and 2.09 Å, as given in Table 2. The N1−Pd−N2 angle is 82.9°, the slight distortion from a perfect square geometry being imposed by the ethylenediamine chelating ligand. The S1−Pd−S4 angle is 89.7°, typical for this kind of complexes.[1,3,18−20] The metal atom lies 0.08 Å above the plane of the four ligands, which is in agreement with the observations regarding the aforementioned complexes.

Table 2. Selected Bond Lengths [Å] and Angles [deg] for $[Pd(ttcn)en](PF_6)_2$ and $[Pt(ttcn)en](PF_6)_2$[a]

$[Pd(ttcn)en](PF_6)_2$		$[Pt(ttcn)en](PF_6)_2$	
bond	distance	bond	distance
Pd−S1	2.263(1)	Pt1−N11	2.058(6)
Pd−S4	2.257(1)	Pt1−N12	2.082(6)
Pd−N1	2.085(4)	Pt1−S11	2.266(2)
Pd−N2	2.078(4)	Pt1−S14	2.259(2)
Pd---S7	3.00	Pt1---S17	3.01
		Pt2−N21	2.085(5)
		Pt2−N22	2.074(5)
		Pt2−S21	2.255(2)
		Pt2−S24	2.265(2)
		Pt2---S27	3.06
$[Pd(ttcn)en](PF_6)_2$		$[Pt(ttcn)en](PF_6)_2$	
bonds defining angle	angle	bonds defining angle	angle
N1−Pd−S1	93.9(1)	N11−Pt1−S11	94.1(2)
N1−Pd−S4	174.6(1)	N11−Pt1−S14	172.3(2)
N2−Pd−S4	93.5(1)	N12−Pt1−S14	94.0(2)
N2−Pd−S1	174.0(1)	N12−Pt1−S11	176.2(2)
S1−Pd−S4	89.7(1)	S11−Pt1−S14	89.8(1)
N1−Pd−S7	102.3(1)	N11−Pt1−S17	102.5(1)
N2−Pd−S7	103.2(1)	N12−Pt1−S17	96.1(1)
S1−Pd−S7	82.3(1)	S11−Pt1−S17	84.2(1)
S4−Pd−S7	82.1(1)	S14−Pt1−S17	80.0(1)
		N21−Pt2−N22	82.6(2)
		N21−Pt2−S21	92.8(2)
		N21−Pt2−S24	175.2(2)
		N22−Pt2−S24	94.1(2)
		N22−Pt2−S21	174.4(2)
		S21−Pt2−S24	90.3(1)
		N21−Pt2−S27	104.0(1)
		N22−Pt2−S27	101.3(1)
		S21−Pt2−S27	83.0(1)
		S24−Pt2−S27	84.5(1)

[a]Estimated standard deviations in the least significant digits are given in parentheses.

3.2. Crystal Structure of $[Pt(ttcn)en](PF_6)_2$. The single crystal X-ray diffraction of $[Pt(ttcn)en](PF_6)_2$ was determined at 293 K. This compound crystallizes in the *Pbca* space group, with $Z = 16$ (see Table 1). There are two crystallographically inequivalent complex molecules and two crystallographically inequivalent sets of two hexafluorophosphate anions in the unit cell. The structure of the $[Pt(ttcn)en]^{2+}$ ion in Figure 1 is similar to that of the palladium(II) analogue, a distorted square-planar geometry with a $Pt---S_{apical}$ interaction resulting in an effective five-coordinate metal. Two of the PF_6^- ions are disordered and resolved into two orientations. There are no significant intermolecular interactions, similar to the palladium(II) complex. The metal−ligand distances for $[Pt(ttcn)en](PF_6)_2$ are given in Table 2 and summarized in Table 3 for the other complexes studied, illustrating typical values for bond lengths and metal-S_{apical} distance for this category of complexes. The axial metal−sulfur distance is 3.01 Å, short enough to consider a metal-apical ligand interaction. In this complex too this axial interaction causes the metal atom to exit the coordination plane by 0.06 Å for Pt1 and 0.07 Å for Pt2.

3.3. Pressure-Dependent Luminescence Spectroscopy. Figures 2 and 3 display representative pressure-dependent

(26) Troullier, N.; Martins, J. L. *Phys. Rev. B* **1991**, *43*, 1993.
(27) Kleinman, L.; Bylander, D. M. *Phys. Rev. Lett.* **1982**, *48*, 1425.
(28) Louie, S. G.; Froyen, S.; Cohen, M. L. *Phys. Rev. B* **1982**, *26*, 1738.

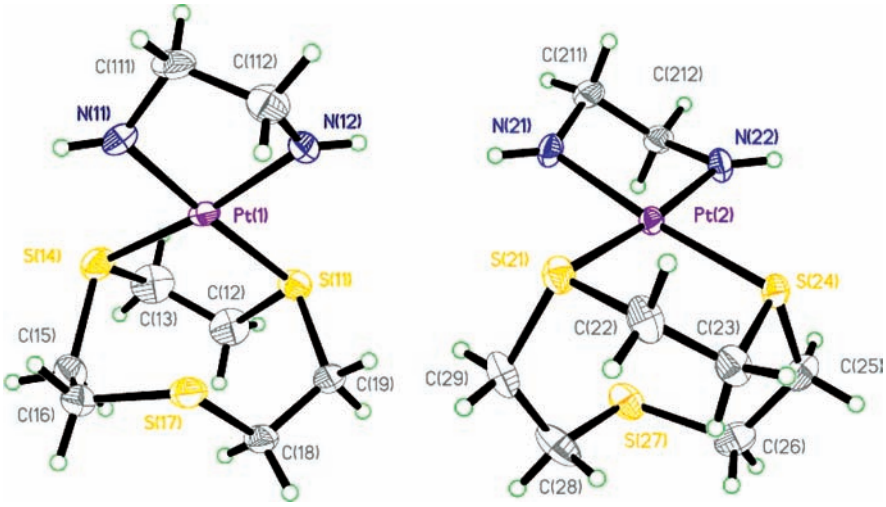

Figure 1. View of the two crystallographically inequivalent $[Pt(ttcn)en]^{2+}$ ions in $[Pt(ttcn)en](PF_6)_2$ showing the labeling scheme. Thermal ellipsoids are shown at the 30% level.

Table 3. Important Intramolecular Distances (Å)

				[Pt(ttcn)en](PF$_6$)$_2$	
	[Pd(ttcn)Cl$_2$][a]	[Pt(ttcn)Cl$_2$][b]	[Pd(ttcn)en](PF$_6$)$_2$	site 1	site 2
M−S$_{equat}$1	2.25	2.221	2.257	2.259	2.255
M−S$_{equat}$2	2.261	2.238	2.263	2.266	2.265
M−S$_{apical}$	3.159	3.26	3.003	3.01	3.06
x	0.10	0.08	0.08	0.06	0.07
d	0.904	1.031	0.743	0.748	0.80

[a] Ref 4. [b] Ref 19.

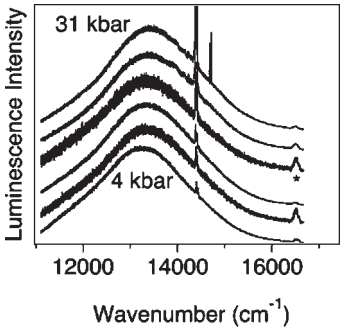

Figure 2. Representative pressure-dependent luminescence spectra for [Pd(ttcn)Cl$_2$] at 4 kbar (bottom), 17, 21, 24, 27, and 31 kbar (top). The spectra are normalized and drawn with an offset along the vertical axis for clarity. A Raman peak is visible at approximately 16500 cm^{-1} and denoted by the asterisk.

spectra of [Pd(ttcn)Cl$_2$] and of both platinum(II) compounds. All title compounds have a broad luminescence band, spanning up to 5000 cm^{-1}. Low luminescence intensity is a common trait for all three compounds, as expected for the doubly forbidden $^1A_{1g} \leftarrow {}^3E_g$ d-d transition (in idealized D_{4h} geometry). These weak bands are hard to measure because any luminescent imperfections or minority sites have a strong influence on the spectra. The room-temperature luminescence intensity of [Pd(ttcn)en](PF$_6$)$_2$ is so low that it was not possible to record pressure-dependent spectra for this complex. A spectrum recorded at 80 K is given in the Supporting Information, Figure S5. Figure 2 shows a peak at approximately 16500 cm^{-1}, corresponding to a Raman band and illustrating the low luminescence

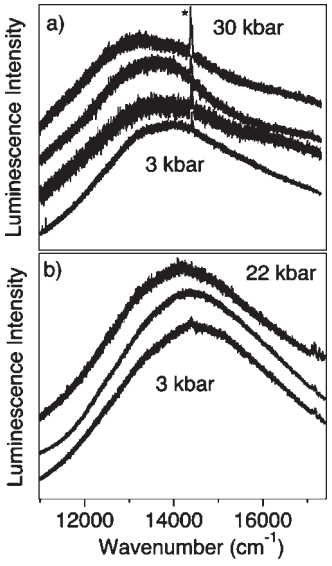

Figure 3. Representative pressure-dependent luminescence spectra for (a) [Pt(ttcn)Cl$_2$] at 3 kbar (bottom), 15, 25, and 30 kbar (top) and (b) [Pt(ttcn)en](PF$_6$)$_2$ at 3 kbar (bottom), 17 and 22 kbar (top). The spectra are normalized and drawn with an offset along the vertical axis for clarity and the sharp peaks denoted by the asterisk in Figure 3a are ruby luminescence.

intensities of the title complexes. The sharp signals at approximately 14500 cm^{-1} observed in some spectra originate from ruby, and we were not able to eliminate them despite using the imaging capabilities of the Raman microscope, again typical for the weak luminescence signals. The

Table 4. Ambient-Pressure Luminescence Parameters

	E_{max} (cm^{-1})	width at half height (cm^{-1})
$[Pd(ttcn)Cl_2]$	13200	1500
$[Pt(ttcn)Cl_2]$	13930	≈ 2400
$[Pd(ttcn)en](PF_6)_2$	≈ 14900	≈ 2200[a]
$[Pt(ttcn)en](PF_6)_2$	14980	≈ 2500

[a]Measured at 80 K.

widths, overall shapes, and intensities of the luminescence bands show continuous and reversible change over the studied pressure range, indicating that the observed transition is always of the same type and that the molecular structure of the compounds is not strongly modified in the process. This is confirmed by the pressure-dependent Raman spectra of the complexes.

The luminescence band maxima at ambient pressure are located at 13300 cm^{-1} for $[Pd(ttcn)Cl_2]$, 14000 cm^{-1} for $[Pt(ttcn)Cl_2]$ and 14500 cm^{-1} for $[Pt(ttcn)en](PF_6)_2$ (Table 4). These values are comparable to those reported for square-planar palladium(II) and platinum(II) compounds with sulfur donor ligands.[12−14,29−32] It is a common trend that the luminescence energies of square-planar platinum(II) complexes are higher than those of their palladium(II) counterparts. The spectra in Figures 2 and 3 show that this trend can be extended to the pseudo square-planar complexes with ttcn ligands described here. Luminescence maxima were determined with least-squares fits of a Gaussian profile to the intensities corresponding to the top 20% region of the luminescence band.

Figures 2 and 3 show that the luminescence band maxima E_{max} are shifted as pressure is increased. All luminescence maxima are shown in Figure 4. Lines are calculated and shown to illustrate trends. $[Pd(ttcn)Cl_2]$ has a +6 cm^{-1}/kbar blue-shift, whereas $[Pt(ttcn)Cl_2]$ and $[Pt(ttcn)en](PF_6)_2$ show red-shifts of −19 cm^{-1}/kbar and −26 cm^{-1}/kbar, respectively, as summarized in Figure 4. Low luminescence intensities and possibly non-hydrostatic pressure gradients leading to different contributions from inequivalent complexes present in $[Pt(ttcn)en](PF_6)_2$ as illustrated in Figure 1 are the cause of the scatter of the observed band maxima. Varying maxima were sometimes observed for different regions of the same sample, at identical nominal pressure, indicative of a significant effect of pressure gradients for this category of complexes. Despite these experimental uncertainties, the surprising qualitative difference between the platinum(II) complexes, which show a red shift, and the palladium(II) complex, which shows a blue shift, is obvious from the data in Figure 4.

To the best of our knowledge, no published report shows opposite shifts of luminescence maxima with pressure for closely related palladium(II) and platinum(II) complexes. The square-planar tetrathiocyanato and tetraselenocyanato palladium(II) and platinum(II) complexes show pressure-induced blue-shifts for both metals,[13−15] as do palladium(II) and platinum(II) dithiocarbamate complexes.[12] This difference is rationalized with theoretical models in the discussion.

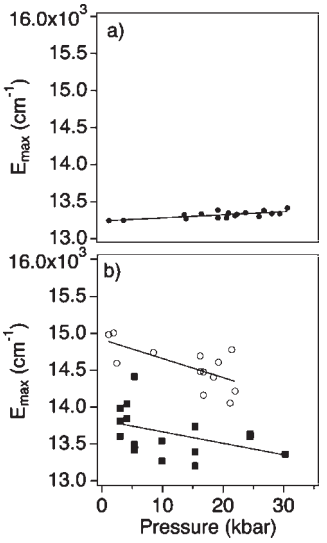

Figure 4. Pressure-induced variation of luminescence band maxima E_{max}: (a) $[Pd(ttcn)Cl_2]$, (b) $[Pt(ttcn)Cl_2]$ (squares) and $[Pt(ttcn)en](PF_6)_2$ (circles). The solid lines represent linear least-squares fits and are shown as a guide for the eye to illustrate the trends.

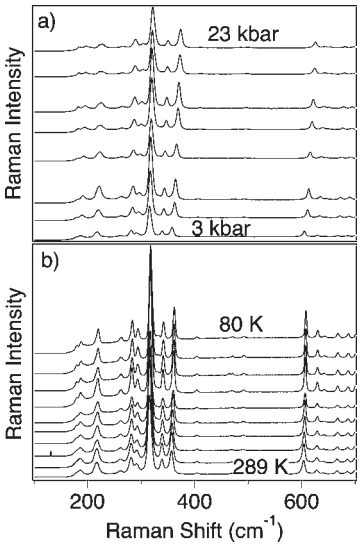

Figure 5. (a) Pressure-dependent Raman spectra of $[Pd(ttcn)Cl_2]$ at 3 kbar (bottom), 9, 12, 14, 16, 19, 21, and 23 kbar (top). (b) Temperature-dependent Raman spectra of $[Pd(ttcn)Cl_2]$ at 80 K (top), 105, 130, 155, 180, 205, 230, 255, 280, and 289 K (bottom).

3.4. Pressure-Dependent Raman Spectroscopy. Pressure-dependent Raman spectra have been recorded for $[Pd(ttcn)Cl_2]$, $[Pt(ttcn)Cl_2]$, and $[Pt(ttcn)(en)](PF_6)_2$. Figure 5a displays the spectra for $[Pd(ttcn)Cl_2]$. Vibrational frequencies in the 300 cm^{-1} range are likely to correspond to metal−ligand stretching modes, as measured at 329 cm^{-1} and 307 cm^{-1} in the Raman spectra of $[PtCl_4]^{2-}$ [31] and $[PdCl_4]^{2-}$,[33] respectively, and assigned to the totally symmetric stretching mode. The corresponding experimental frequencies are 303 cm^{-1} and 274 cm^{-1} for $[Pt(SCN)_4]^{2-}$ and $[Pd(SCN)_4]^{2-}$,[34] respectively, lower in frequency by

(29) Pelletier, Y.; Reber, C. *Inorg. Chem.* **1997**, *36*, 72.
(30) Pelletier, Y.; Reber, C. *Inorg. Chem.* **2000**, *39*, 4535.
(31) Preston, D. M.; Güntner, W.; Lechner, A.; Gliemann, G.; Zink, J. I. *J. Am. Chem. Soc.* **1988**, *110*, 562.
(32) Reber, C.; Grey, J. K.; Lanthier, E.; Frantzen, K. A. *Comments Inorg. Chem.* **2005**, *26*, 233.
(33) Chen, Y.; Christensen, D. H.; Nielsen, O. F.; Hyldtoft, J.; Jacobsen, C. J. H. *Spectrochim. Acta* **1995**, *51A*, 595.
(34) Rohde, J.-U.; von Malottki, B.; Preetz, W. *Z. Anorg. Allg. Chem.* **2000**, *626*, 905.

20−30 cm^{-1} for the palladium(II) complexes compared to their platinum(II) analogues. Several Raman active stretching frequencies are expected for the title compounds, as their symmetry is lower and the ligands are not identical. The experimental spectrum of [Pd(ttcn)Cl_2] in Figure 5 shows two prominent peaks at 316 cm^{-1} and 339 cm^{-1}, most likely corresponding to metal−ligand stretching modes. Corresponding frequencies in the spectra of [Pt(ttcn)Cl_2] and [Pt(ttcn)(en)]$(PF_6)_2$ are 388 cm^{-1} and 362 cm^{-1}, again likely corresponding to metal−ligand stretching modes. These assignments are supported by DFT calculated Raman spectra for isolated molecules. Calculated and experimental Raman spectra of [Pt(ttcn)Cl_2] and [Pd(ttcn)Cl_2] are compared in the Supporting Information, Figure S7. Calculated frequencies tend to be lower than experimental values from Raman spectra. For $[PtCl_4]^{2-}$ and $[PdCl_4]^{2-}$, stretching frequencies of 268 cm^{-1} and 245 cm^{-1} were calculated,[35] lower than the experimental values by 61 cm^{-1} and 59 cm^{-1}, respectively. Similar differences of 54 cm^{-1} and 50 cm^{-1} were obtained between calculated and observed frequencies for $[Pt(SCN)_4]^{2-}$ and $[Pd(SCN)_4]^{2-}$.[35] Normal coordinates with metal−ligand stretching character correspond to the calculated frequencies of 320 cm^{-1} and 297 cm^{-1} for [Pt(ttcn)Cl_2] and [Pd(ttcn)Cl_2]. The experimental peaks observed at 316 cm^{-1} and 342 cm^{-1} for [Pd(ttcn)Cl_2] in the spectra illustrated in Figure 5 are therefore likely to correspond to metal−ligand stretching modes. The temperature-dependent spectra in Figure 5b indicate that these frequencies show a linear decrease of −0.015 cm^{-1}/K with decreasing temperature. The spectra recorded at variable pressure in Figure 5a show frequency increases of +0.27 cm^{-1}/kbar and +0.49 cm^{-1}/kbar for the maxima at 316 cm^{-1} and 342 cm^{-1}, respectively. These values are comparable to the corresponding peaks of [Pt(ttcn)Cl_2] at 355 cm^{-1} and 389 cm^{-1}, where increases by +0.51 cm^{-1}/kbar and +0.63 cm^{-1}/kbar were observed. The similar pressure variations and comparable differences to calculated frequencies can therefore be used to assign these peaks to metal−ligand stretching modes. The corresponding peak at 362 cm^{-1} for [Pt(ttcn)(en)]$(PF_6)_2$ shows a pressure-induced increase of only +0.08 cm^{-1}/kbar, possibly a consequence of the chelating ethylenediamine ligand preventing pressure-induced structure changes to a larger extent than the monodentate chloro ligands. The comparison of experimental and calculated frequencies therefore allows the metal−ligand stretching modes to be identified and reveals characteristic differences between the two platinum(II) complexes.

The Raman spectra in Figure 5 and in the Supporting Information provide essential experimental information indicating that the crystals do not disastrously deteriorate as pressure increases, a situation that would prevent any analysis of the luminescence spectra. The number and shape of the Raman bands are conserved over the studied pressure range, and only very small frequency shifts are observed, as both pressure or temperature are varied, shown in Figures 5a and 5b, respectively. This is a strong indication that the crystal packing and the overall molecular structure of the complex are retained as pressure is increased.

(35) Lanthier, E.; Reber, C.; Carrington, T., Jr. *Chem. Phys.* **2006**, *329*, 90.

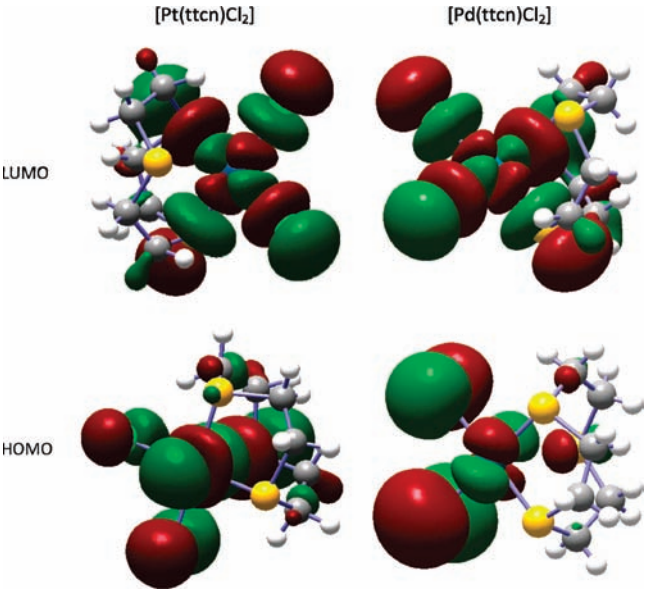

Figure 6. Calculated frontier molecular orbitals for [Pt(ttcn)Cl_2] (lefthand column) and [Pd(ttcn)Cl_2] (righthand column). The LUMO (top row) have identical $d_{x^2-y^2}$ character, but the d-orbital contributions to the HOMO (bottom row) are different: d_{z^2} for [Pt(ttcn)Cl_2] and d_{xz} for [Pd(ttcn)Cl_2].

4. Discussion

4.1. Assignment of Luminescence Transitions. The energies and band widths of the observed bands are similar to those of sulfur-coordinated square-planar platinum(II) and palladium(II) complexes, where the d-d character of the luminescence transition has been clearly confirmed.[12−15,30,32,36] The weak luminescence signals observed for the title complexes are also typical for d-d transitions. The solution absorption spectra show molar absorptivities of less than 100 $M^{-1}cm^{-1}$ in the 20000 cm^{-1} to 30000 cm^{-1} range, again in agreement with a d-d assignment. The spectrum of $[Pt(ttcn)en]^{2+}$ is shown as a representative example in the Supporting Information. Raman spectra do not show resonance enhancements as the molar absorptivities in the visible wavelength range are too low.

DFT calculations are used to support this assignment and to obtain information on the HOMO and LUMO. The latter is expected to be the σ^* orbital with a significant $d_{x^2-y^2}$ contribution from the metal center, confirmed for both [Pd(ttcn)Cl_2] and [Pt(ttcn)Cl_2] as shown in Figure 6. The highest energy occupied orbitals are close in energy for square-planar complexes, and their order can be different even for platinum(II) and palladium(II) compounds with identical ligand spheres.[37,38] The shapes of HOMO for both [Pd(ttcn)Cl_2] and [Pt(ttcn)Cl_2] are also given in Figure 6. Figure 7a shows calculated orbital energy levels for optimized molecular structures of single [Pd(ttcn)Cl_2] and [Pt(ttcn)Cl_2] complexes. Energy differences between LUMO and HOMO are 15700 cm^{-1} and 13350 cm^{-1} for [Pt(ttcn)Cl_2] and [Pd(ttcn)Cl_2], respectively. The platinum(II) compound has a calculated energy difference higher by approximately 2000 cm^{-1} than the palladium(II) analogue, comparable to the energies of

(36) Güntner, W.; Gliemann, G.; Kunkely, H.; Reber, C.; Zink, J. I. *Inorg. Chem.* **1990**, *29*, 5238.
(37) Deeth, R. J. *Faraday Discuss.* **2003**, *124*, 379.
(38) Harvey, P. D.; Reber, C. *Can. J. Chem.* **1999**, *77*, 16.

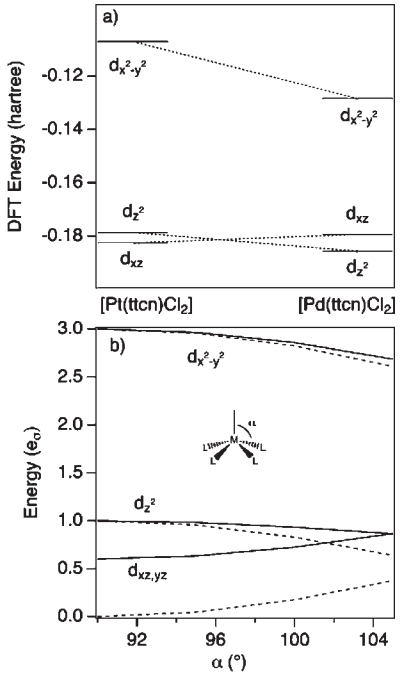

Figure 7. (a) Calculated HOMO-1, HOMO, and LUMO molecular orbital energies for $[Pd(ttcn)Cl_2]$ (left) and $[Pt(ttcn)Cl_2]$ (right). The character of the main contributing metal d-orbital is indicated. (b) Angular overlap calculations illustrating the effect of the out-of-plane distance of the metal ion, represented by the angle α, on the HOMO-1, HOMO, and LUMO molecular orbital energies for a square-planar complex with four identical ligands. Solid lines are calculated for an e_π/e_σ ratio of 0.3, dotted line for a ratio of 0.

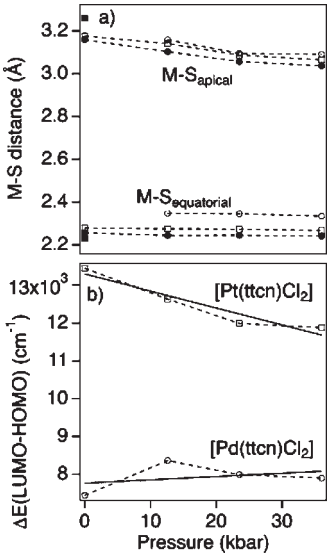

Figure 8. (a) Experimental and calculated metal-S distances. Experimental values for $[Pd(ttcn)Cl_2]$ are from the pressure-dependent structures in ref 4 and are shown as solid circles. Experimental values for $[Pt(ttcn)Cl_2]$ at ambient pressure are shown as solid squares. Calculated values using the SIESTA program for $[Pd(ttcn)Cl_2]$ and $[Pt(ttcn)Cl_2]$ are denoted by open circles and squares, respectively. (b) Calculated LUMO−HOMO energy differences for $[Pd(ttcn)Cl_2]$ (circles) and $[Pt(ttcn)Cl_2]$ (squares).

the luminescence maxima in Figures 2 and 3, where the emission maximum for $[Pt(ttcn)Cl_2]$ is higher by approximately 1000 cm^{-1} than for $[Pd(ttcn)Cl_2]$ at ambient pressure. The calculations show the d_{z^2} orbital providing a significant contribution to the HOMO for $[Pt(ttcn)Cl_2]$, and the HOMO-1 for this complex involves the d_{xz} metal orbital. In contrast, the d_{xz} orbital provides the dominant contribution to the HOMO in $[Pd(ttcn)Cl_2]$, with the d_{z^2} orbital lower in energy (HOMO-1). The calculations indicate that the metal-S_{apical} interaction in $[Pt(ttcn)Cl_2]$ is strong enough to destabilize the d_{z^2} orbital above the other occupied d-orbitals. In $[Pd(ttcn)Cl_2]$, this is not the case. One reason for this is the out-of-plane distance x of the metal center. The experimental values in Table 3 show that palladium(II) complexes always have larger x values than their platinum(II) analogues, independent of the ligands completing the square-planar coordination sphere. This trend of the out-of-plane distances x is also obtained from the optimized calculated geometries for single molecules.

The influence of the out-of-plane distance x on the energy order of the HOMO-1, HOMO, and LUMO can be probed with idealized symmetry and the angular overlap model. Figure 7b illustrates this approach. We use four identical ligands in a square-planar structure and increase their angle α with the z axis perpendicular to the molecular plane, corresponding to an increase of the out-of-plane distance x of the metal center. At small angles, d_{z^2} is the HOMO, as calculated for the platinum(II) complexes, but at large angles, d_{xz} is higher in energy, as calculated for the palladium(II) complexes. Strong π−donor ligands emphasize this trend, as illustrated by the trends shown for a high value of the e_π/e_σ ratio, appropriate for the ligands of the two complexes for which calculations were carried out. The angular overlap approach therefore provides qualitative support for the orbital energy order obtained by DFT calculations.

4.2. Pressure Effects. The luminescence maxima shift in different directions for $[Pd(ttcn)Cl_2]$ and $[Pt(ttcn)Cl_2]$ as pressure increases. In square planar complexes without apical ligands, a blue shift is observed for d-d luminescence bands.[12−14,32,38] It is caused by the stronger destabilization of the σ^* LUMO compared to the π^* HOMO, both in square-planar and octahedral complexes. In contrast, pressure-induced red-shifts are observed in platinum(II) complexes with strong axial interactions, involving platinum(II) ions in stacked structures or other neighboring groups.[16,39] The platinum(II) complexes studied here show a dominant effect of the axial interaction, leading to a strong increase of the Pt−S_{apical} σ^* d_{z^2} HOMO, dominating the energy increase of the LUMO, and therefore resulting in a red shift.

In the palladium(II) complex, the HOMO is calculated to be d_{xz}, the same as for square-planar complexes without pendant nucleophiles. The pressure-induced decrease of the Pd−S_{apical} distance destabilizes the π^* HOMO to a lesser extent than the σ^* HOMO of the platinum(II) complexes. It appears that the destabilization of the HOMO is not sufficient to dominate the effect of pressure on LUMO, and the weak blue shift illustrated in Figure 4a results.

$[Pd(ttcn)Cl_2]$ is one of only a few complexes for which pressure-dependent crystal structures have been reported.[4] Figure 7a summarizes the effect of pressure on Pd−S_{apical} and Pd−$S_{equatoral}$ distances. The Pd−S_{apical} distance decreases by 0.2 Å between ambient pressure and 30 kbar. In contrast, the effect on the equatorial bonds is smaller by an order of magnitude. SIESTA calculations lead to calculated

(39) Levasseur-Thériault, G.; Reber, C.; Aronica, C.; Luneau, D. *Inorg. Chem.* **2006**, *45*, 2379.

structures and orbital energies as a function of pressure. The calculated structures can be compared to the experimental data for [Pd(ttcn)Cl_2] and effects for the [Pt(ttcn)Cl_2] can be calculated. Figure 8a shows that calculated Pd−S distances are in good agreement with the experimental values. For [Pt(ttcn)Cl_2], similar trends are calculated, with reasonable agreement with the ambient-pressure values also given in this Figure. Calculated HOMO−LUMO energy differences are shown in Figure 8b. It is interesting to note that an excellent qualitative agreement with the experimental results is obtained. For [Pd(ttcn)Cl_2], the calculated energy difference increases by $+10$ cm^{-1}/kbar, and for [Pt(ttcn)Cl_2] a decrease by -45 cm^{-1}/kbar is calculated, as shown by the best-fit lines in Figure 8b. This comparison shows that DFT calculations of the type used here can be applied to rationalize the influence of weaker effects, such as the metal-S_{apical} distances, on d-d electronic transitions, as illustrated by the luminescence spectra.

Acknowledgment. The authors thank Professor William B. Connick (University of Cincinnati) for bringing this category of compounds to our attention and Francine Bélanger-Gariépy (Université de Montréal) for help with the crystal structure determination. Financial support from the Natural Sciences and Engineering Research Council (Canada), the Région Rhône-Alpes and the Commissariat à l'Énergie Atomique (CEA) through a Laboratoire de Recherche Conventionné (LRC CEA No DSM-03-31) is gratefully acknowledged.

Supporting Information Available: Raman spectra of [Pt(ttcn)en]$(PF_6)_2$ and [Pt(ttcn)Cl_2] as a function of pressure and temperature, comparison of calculated and experimental Raman spectra for [Pt(ttcn)Cl_2] and [Pd(ttcn)Cl_2], X-ray crystallographic file in CIF format for [Pd(ttcn)en]$(PF_6)_2$ and [Pt(ttcn)en]$(PF_6)_2$. This material is available free of charge via the Internet at http://pubs.acs.org.